STUDIES ON IMPROVEMENT OF NONLINEAR PITCHING MOMENT CHARACTERISTICS OF CRANKED-ARROW WING

Weiheng ZHAO*, Dongyoun KWAK and Kenichi RINOIE***
***Department of Aeronautics and Astronautics,**
University of Tokyo, 113-8656, JAPAN
****Japan Aerospace Exploration Agency, 181-0015, JAPAN**

Keywords: *Cranked-Arrow Wing, High angle of Attack, Pitching Moment, Vortex Breakdown*

Abstract

A series of low speed wind-tunnel tests have been conducted to improve the non-linear pitching moment characteristics of a cranked-arrow wing configuration at high angle of attack. Aerodynamic forces were measured, and flow fields were visualized by the oil flow technique and smoke visualization. Results indicate that the non-linear phenomena obtained on the pitching moment occur at high angles of attack which are corresponded with the take-off and landing flight conditions. These non-linear pitching moment characteristics are caused by the outboard wing separation and the inboard vortex breakdown, respectively. Several aerodynamic devices have been equipped on the baseline configuration to improve the non-linear characteristics. The leading-edge flap deflection and pylon-shaped vortex generator could improve the non-linear characteristics effectively by the suppression of the outboard flow separation and enforcement of inboard leading-edge vortex. The improvements by these devices were also discussed with the low speed aerodynamic performance taken into account. Relationship between the rate of non-linear characteristics and maximum lift to drag ratio (L/D) shows that the leading-edge flap could improve both non-linear problem and L/D, while the pylon-shaped vortex generator suffer drag penalty despite of its improvement effects.

Nomenclature

S	wing area, m^2
b	length of maximum wing span, m
C_{root}	length of wing root chord at center-line of the model, m
C_{tip}	length of wing tip, m
C_{mac}	wing mean aerodynamic chord, m
Re	Reynolds Number based on mean aerodynamic chord
U_∞	free stream velocity m/s
x	chord wise coordinate measured from apex of the cranked-arrow wing at model center line, m
y	span wise coordinate orthogonal to x, fix to the body and measured from center line, m
z	coordinate orthogonal to x and y, fix to the body and measured from center line, m
ξ	dimensionless coordinate of x based on wing root chord
η	dimensionless coordinate of y based on wing semi-span
α	angle of attack, deg
C_L	lift coefficient
C_D	drag coefficient
C_m	pitching moment coefficient, reference point at 25% mean aerodynamic chord (See Fig.7)
L/D	lift / drag ratio
$C_{m\alpha}$	slope of pitching moment coefficient
C_{D0}	parasite drag

N_0 dimensionless neutral point of the wing based on mean aerodynamic chord, defined in equation (1)

ΔN_0 variable to measure the rate of non-linear pitching moment characteristics, defined in equation (2)

1. Introduction

The cranked-arrow wing is one of the suitable wing configurations for supersonic transport (SST). The low aspect ratio and highly swept wing platform can lead to relevant performance at supersonic flight regime, while higher lift and lift to drag ratio were required at high alpha flight conditions to improve the take-off and landing performance. At high alpha flight regime, the leading-edge separation vortices are formed over the wing [1]. These vortices can induce the suction force which is called vortex lift [1]. However, behaviors of the separation vortices are very complicated, which potentially causes some negative effects.

One of the major issues for low speed aerodynamics of the cranked arrow wing configuration is the non-linear pitching moment characteristics which caused abrupt increment of $C_{m\alpha}$ that result in the loss of longitudinal stability at high angle of attack [2]. Since the angles of attack where the non-linear pitching moment occurred corresponds to that at take-off and landing flight regime, it could destabilize and threaten the aircraft. Therefore, understanding the mechanism of the non-linear pitching moment C_m characteristics is an important task to improve the low-speed performance of the SST.

In general, the non-linear C_m characteristics are considered to be composite effects of three aerodynamic phenomena caused by leading-edge separation vortex:

- flow separation of outboard wing [3].
- breakdown of leading-edge vortex [4] [5].
- interaction of inboard and outboard vortex [4] [5].

The behaviors of these phenomena are complicated and strongly affected by the design parameters of the wing platform (for example, sweep back angle, kink position) [6]. However, since these parameters are settled by supersonic performance requirements of the aircraft, it is not reasonable to change them for low speed purpose. Therefore, it is necessary to improve the non-linear characteristics by small change of the wing platform.

From previous researches, it has been found that longitudinal destabilization of delta wing configuration is able to be improved by equipping aerodynamic devices to the platform [7] [8]. These suggest that the non-linear pitching moment of the cranked-arrow wing platform might be resolved by equipping adequate devices that do not dramatically change the configuration.

In this research, a series of wind tunnel tests have been conducted to investigate characteristics of the non-linear pitching moment for a cranked-arrow wing configuration. Relationship between the aerodynamics and flow behaviors was analyzed by force measurement and flow visitation. Several aerodynamic devices were introduced to improve the non-linear characteristics. Effects of improvement were analyzed at preliminary phase. Some devices indicated large gains were chosen and were investigated in detail at second phase. Influences on low speed aerodynamics (i.e. *L/D*) were also discussed.

2 Experimental Details

The experiments presented in this paper are performed by two series of wind tunnel tests: preliminary wind tunnel tests and detailed wind tunnel tests. The purpose of preliminary tests was to point out what kind of devices seem to have improvement effects by relatively rough measurements. On the other hand, the detailed tests were to understand the mechanisms of the non-linear pitching moment and effects of the devices which shown improvements in preliminary tests by accurate measurements. The preliminary tests were conducted using a wind tunnel in university of Tokyo, as well as, the detailed tests were conducted in a JAXA wind tunnel.

2.1 Wind tunnel test in university of Tokyo

The preliminary tests were conducted in a 0.6m×0.6m blow-down low speed wind tunnel located at Department of Aeronautics and Astronautics, University of Tokyo (Fig.1). Force measurement and smoke flow visualization were made at Re = 9.6×10^4, 6.8×10^4, respectively. Lift, drag and pitching moment have been measured by an external balance. Behaviors of flow field at several cross sections perpendicular to coordinate ξ were visualized by smoke and light sheet technique (Fig.3). Locations of the inboard vortex breakdown onset, which is defined as the average value of the ξ where vortex core is clear and the ξ where vortex core is completely disappeared, was measured. This is because the vortex breakdown location slightly oscillated along the vortex axis direction.

Figure 5 shows the baseline configuration of the cranked-arrow wing and tested configuration with several aerodynamic devices equipped. The baseline configuration used in preliminary tests is a 1/5 scaled model of that used in JAXA tests. The S and the C_{mac} of the baseline model are 0.01166m^2 and 0.0854m. Effects of the five aerodynamic devices, which are shown in Fig.5, were investigated by comparing the C_m-α and smoke flow fields.

2.2 JAXA wind tunnel tests

The detailed tests were conducted in the 2.0m×2.0m circuit low speed wind tunnel located at Japan Aerospace Exploration Agency (JAXA) (Fig.2). Six components aerodynamic force measurement and flow visualization by the oil flow technique have been made at Re = 9.1×10^5 (Fig.4). Aerodynamic coefficients (i.e. C_L, C_D and C_m at 55% C_{root}) were measured in the range of α = -4° to 30° (Fig.6). Figure 7 shows the baseline configuration of the cranked arrow wing with fuselage used in JAXA wind tunnel tests. The wing is a flat plate with a sharp edge as shown in Fig.7. The S and C_{mac} of the model are 0.293m^2 and 0.459m. The wing areas enclosed by blue lines are removable parts where aerodynamic devices could be equipped from the baseline. The areas enclosed by red lines are the leading-edge vortex flap and the trailing-edge flap that can be set to arbitrary deflection angles.

Figure 8 to 11 show four configurations with aerodynamic devices equipped. Short name of these configurations are defined as: lift surface increment:"LS" (Fig.8), kink smoothing:"KS", (Fig.9), leading-edge flap deflection:"LE-flap" (Fig.10) and pylon-shaped vortex generator:"VG" (Fig.11). These four configurations had indicated large improvements for the non-linear characteristics from the preliminary tests. These were selected to investigate in detailed tests.

The definition of the LE-flap is based on Rao and Rinoie's segmented vortex flaps presented in Ref.9 and 10. The leading-edge flaps consisted of 4 segments on a half wing, as shown in Fig.10. The deflection angles of these segments can be set independently. In this paper, the flap deflection angles of each segment are presented as "LE-flap $\delta_{(i)}$- $\delta_{(ii)}$- $\delta_{(iii)}$- $\delta_{(iv)}$" (The "$\delta_{(i)}$" stands for the flap down deflection angle of the segment (i), as shown in Fig.10). For example, "LE-flap 30-35-10-15" means the flap down deflection angles of segment (i), (ii), (iii), (iv) are 30°, 35°, 10° and 15°, respectively.

The configuration of the "VG" is based on Rao's pylon-shaped vortex generator in Ref.8. The previous paper was reported that a delta wing with "VG" installed had shown improvement of longitudinal instability. The "VG" shape in this research was chosen a similar shape from Ref.8. Effects of the "VG" with different size is also tested (Fig.11). Installation locations and numbers of the VG are defined by coordinate η, as shown in Fig.11. For example, "VG η=0.2, 0.68" means two VG are installed at η=0.2 and 0.68 on a half wing.

The non-linear characteristics of each configuration are accessed by observing changes of C_m-α curve and neutral point N_0. The dimensionless neutral point N_0 based on mean aerodynamic chord is represented as following equation (1):

$$N_0 = \frac{1}{4} - \frac{dC_m}{dC_L} \qquad (1)$$

An obvious non-linear characteristic can present by an abrupt change in N_0. Thus the

non-linear characteristics of C_m-α curves at α=0° to 25° for each device can be assessed quantitatively by the difference of maximum and minimum of N_0. Thus, the variable ΔN_0 is introduced to characterize the strength of the non-linear characteristics, which is represented as equation (2) (Fig.19 (b)):

$$\Delta N_0 = max(N_0) - min(N_0) \quad (2)$$

$$At \ \ \alpha <= 0° \ to \ 25°$$

3 Results and Discussion

3.1 Results on the preliminary tests

Figure 12 shows the C_m-α on the baseline configuration and nine configurations with aerodynamic devices which obtained from preliminary tests at $Re = 9.6\times10^4$. Result of the baseline configuration (Fig.12 (a)) indicates the C_m at α<10° is relatively linear. However, further increasing the angles of attack, abrupt changes (i.e. non-linear characteristic) of C_m are observed around α=10°, 14° (i.e. (i) and (ii) in Fig.12 (a)). Since these angles correspond to those adopted by SST at take-off or landing regime, it is necessary to keep the C_m-α linear up to these angles.

The C_m-α curves on other configurations suggest that several devices could improve the non-linear characteristics ("LS": Fig.12 (b), "KS":Fig.12 (c), "LE-flap 30-30-0-0":Fig.12 (d), "LE-flap 0-0-15-15":Fig.12 (e) and "VG η=0.2, 0.4, 0.68": Fig.12 (f)). The "LS" and "VG" seem to improve the overall non-linear characteristics until relatively high angle of attack. However the "KS" and "LE-flap" delay the occurrence of the non-linear C_m.

3.2 Results and Discussion

3.2.1 Mechanism of the Non-linear characteristic for the baseline configuration

Figure 13 shows the C_L-α, C_D-α and L/D-C_L, and Figure 19 shows the C_m-α and N_0-α on the baseline configuration obtained by the JAXA wind tunnel tests at $Re = 9.1\times10^5$. The C_m-α indicates the non-linear pitching moment characteristics occur at two angles of attack α =10° to 12° (i.e. (i) in Fig.19 (a)) and α=13° to 14°(i.e. (ii) in Fig.19 (a)). At these angles of attack, abrupt changes of $C_{m\alpha}$ that destabilize the longitudinal stability are observed. The non-linear characteristics are also reflected as decrement of the magnitude of N_0, which can be seen from N_0-α presented in Fig.19 (b). Slight changes of C_L at same angles of attack are also observed (Fig.13 (a)), which suggest the non-linear characteristics are caused by loss of lift.

Compared to the C_m at $Re = 9.6\times10^4$ (Fig.19 (a)), the absolute value of C_m at $Re = 9.1 \times 10^5$ is lager. This difference of C_m-α curves between $Re = 9.6\times10^4$ and $Re = 9.1\times 10^5$ is mainly caused by the difference of fuselage geometry between two models (the baseline model in detail tests and the model used in preliminary tests). Furthermore, it was suggested that Reynolds number effect also causes the difference. However, the tendency of non-linear characteristics and the angles of attack of which they are observed are almost the same with each other. Therefore it is possible to discuss the non-linear characteristics of the cranked-arrow wing at different Reynolds number.

Figure 30 shows sketches of oil-flow pattern obtained from the detail tests and smoke pictures of vortex feature obtained from the preliminary tests at α=12°, 14° and 16°. It can be observed from Figs.30 (a) and (b) that a region of separation flow begins to form in company with the outboard vortex rising from the surface of wing at 12°. Further increasing the angle of attack up to α =14°, 16°, the outboard vortex significantly lifts-off from the wing surface in accompany with formation of a larger separation region compared to 12° (Figs.30 (c) and (d)). Moreover, the core of inboard vortex become larger, which suggests the vortex start to break down at trailing-edge (Fig.30 (d)). Therefore, analysis on these visualization results can lead to a conclusion that the non-linear characteristics occur at two α (i.e. (i) at α =10° to 12°, (ii) at α =13° to 14°, Fig.19) are owing to loss of lift at trailing-edge

caused by flow separation on outboard wing and inboard vortex breakdown, respectively.

3.2.2 Effects of Lift Surface Increment "LS"

Figure 14 shows the C_L-α, C_D-α and L/D-C_L curves. Figure 20 shows the C_m-α and N_0-α on the "LS" configuration obtained from the JAXA tests. Results of the baseline are also plotted as red lines for comparison. Figure 14 and Fig.20 (a) indicates the absolute values of aerodynamic coefficients (i.e. C_L, C_D and C_m) on the "LS" are larger than those of the baseline. However, the tendency of C_m and N_0 versus α is very similar to that on the baseline (Fig.20). The angles of attack that encounter non-linear characteristics are almost the same with each other. Magnitude of the ΔN_0=0.314 (Fig.36) is also close to that on the baseline (ΔN_0 =0.400). For each figure, a line named "LS_moved" is also presented. The lines of "LS_moved" are estimated from the "LS" results. The transfer of the $0.25C_{mac}$ location caused by increment of the wing area near the trailing edge ("LS") was compensated by shifting the location of the moment center from $0.25C_{mac}$ on the baseline. Result of C_m indicates that the "LS_moved" is almost the same with that of the baseline. Therefore, these facts suggest that the LS only changes the slope of C_m because the additional lift surface on the trailing-edge increases reference area and moves the aerodynamic center to backward of the wing.

Figure 26 shows the result of the chordwise location of the vortex breakdown onset. Figure 31 shows the sketch of flow pattern and smoke picture of vortex feature on the "LS" at α=14° and 16°, respectively. Comparing with the flow pattern on the baseline at same angle of attack (Figs.30 (c) and (d)), hardly any difference can be observed. The breakdown locations in Fig.26 also suggest the result on the "LS" and the baseline are almost the same with each other. Thus it is possible to say that the equipment of the "LS" have little influence on flow field, which means it has hardly any improvement on the non-linear C_m characteristics.

3.2.3 Effects of Kink Smoothing (KS)

Figure 15 shows the C_L-α, C_D-α and L/D-C_L and figure 21 shows the C_m-α and N_0-α of the "KS" configuration obtained from the detail tests. Comparing with the baseline, hardly any changes can be observed from the results of C_L, C_D and L/D (Fig.15). The graph of C_m-α (Fig.21 (a)), on the other hand, suggest that the "KS" delays the non-linear characteristic of (i) (See *3.2.1* and Fig.19) by 3°. However, the magnitude of ΔN_0 is 0.434 (Fig.36), which have little change from the baseline (ΔN_0 = 0.400).

Figure 27 shows the results of the chordwise location of the vortex breakdown onset. Figure 32 shows the sketch of flow pattern and smoke picture of vortex feature on the "KS" at α =14°, 16°. The flow pattern of the "KS" indicates that only inboard vortex is formed on the surface of the wing because the smooth kink obstructs the formation of outboard vortex. However, the region of separation flow (Fig.32 (a)) and the vortex breakdown locations after α =16° (Fig.27) are similar to those of the baseline. Similar trends are also seen form sectional vortex feature at α =14° (Fig.32 (b)). Therefore, the "KS" has only slight improvement on non-linear characteristics.

3.2.4 Effects of Leading-edge Flap Deflection (LE-flap)

Figure 16 shows the C_L-α, C_D-α and L/D-C_L of configurations of the "LE-flap". Results of the C_L-α (Fig.16 (a)) indicate that each "LE-flap" configuration has smaller C_L at α =10° to 16°. However, results of the C_D-α (Fig.16 (b)) suggest the "LE-flap" reduce the drag all over the angles of attack up to 30°. As a result, each "LE-flap" configuration obtains a higher pick of L/D, as shown in Fig.16 (c). The drag reduction effect of the "LE-flap" has been described in Ref.9, 10. That is the deflection of flaps reclines the component of vortex suction force and hence creates a net thrust component, which neutralizes the drag force.

Figure 22 and 23 show the C_m-α, N_0-α of the "LE-flap 30-30-0-0", "LE-flap 0-0-15-15" and "LE-flap 30-30-15-15", "LE-flap 30-35-10-15", respectively. The C_m-α (Fig.22 (a) and Fig.23 (a)) suggest that each "LE-flap"

configuration is able to improve the non-linear characteristics until relatively high angle of attack. The characteristics of N_0-α (Fig.22 (b) and Fig.23 (b)) also reflect the similar trend as the amplitude of N_0 of each LE-flap is smaller than that on the baseline. The ΔN_0 of the "LE-flap" configurations are around 0.14~0.24 (Fig.36), which are smaller than Baseline (ΔN_0=0.400) by approximately 0.2. Investigating the improvement effects of each configuration, it is observed the "LE-flap 0-0-15-15" improves the non-linear characteristic at (i) of the baseline so that extend the linear region until α =16° (Fig.22 (a)). The "LE-flap 30-30-0-0", on the other hand, does not show improvement on non-linear characteristic at (i) but improves the non-linear characteristic at (ii) (Fig.22 (a)). The "LE-flap 30-30-15-15" and the "LE-flap 30-35-10-15" are able to improve both non-linear characteristics at (i) and (ii), thus keep the C_m linear until very high angle of attack (Fig.23 (a)).

Figure 28 shows the result of chordwise location of the vortex breakdown onset. Figure 33 and 34 show the sketches of flow pattern and smoke pictures of vortex feature on each "LE-flap" configuration. The flow pattern of "LE-flap 0-0-10-15" (Fig.33 (a)) at α=12° indicates that outboard vortex is formed on outer side of the wing compared to the baseline (Fig.30 (a)). Region of attached flow are dominative on the outboard wing instead of separated flow observed on the baseline. These results lead to a conclusion that outboard flap deflection can effectively suppresses the separation on outboard wing so that at improve the non-linear characteristic at (i). The flow pattern of "LE-flap 30-35-0-0" (Fig.33 (c)) at α=16° indicates somewhat different phenomena compared with "LE-flap 0-0-10-15". The outboard vortex is smaller and the separation region is larger than that of Baseline (Fig.30 (c)), which suggests that flow separation on outboard wing is even worse. However, the vortex breakdown locations indicate the "LE-flap 30-30-0-0" is able to obstruct the breakdown locations from moving to apex of the wing (Fig.28). This effect is considered to be owing to enforcement of inboard vortex caused by inboard flap deflection. Thus, it is concluded that inboard flap deflection is able to improve the non-linear characteristic at (ii) caused by inboard vortex breakdown. The flow patterns of "LE-flap 30-35-10-15" at α=12°, 16° could be interpreted as combinations of the "LE-flap 30-35-0-0" and "LE-flap 0-0-10-15" (Fig.34). That is, deflection of outboard flaps suppresses separation of outboard wing so that improve the non-linear characteristic at (i). While deflection of inboard flaps obstruct vortex breakdown point from moving to wing apex and consequently improve the non-linear characteristic at (ii).

3.2.5 Effects of Pylon-shaped Vortex Generator (VG)

Figure 17 and 18 show the C_L-α, C_D-α and L/D-C_L of configurations on the pylon-shaped vortex generator "VG". Installation of the "VG" seems to have some negative effects on aerodynamics because they reduce the maximum C_L and increase the CD_0 (Figs.17 (a), (b) and Figs.18 (a), (b)), which result in obvious reduction of maximum L/D (Fig.17 (c) and Fig.18 (c)). Despite of its negative impact on L/D, the non-linear improvement effects are the best among all tested devices. The C_m-α and N_0-α show in Fig.24 and 25 suggest all "VG" configurations can improve the non-linear characteristics on the baseline. The ΔN_0 of the"VG" configurations are smaller than that on the baseline by at the highest 0.3 (Fig.36). Comparing the result of each configuration, it is found the configurations with the "VG" at η=0.68 installed (i.e. "VG η=0.68", "VG η=0.2, 0.68", "VG η=0.4, 0.68" and "VG η=0.2, 0.4, 0.68") show good improvement on non-linear characteristics at both (i) and (ii) (Fig.24 (a)). Configurations without "VG" at η=0.68 (i.e. "VG η=0.2", "VG η=0.2, 0.4", "VG η=0.4"), on the other hand, are somewhat inferior to those with the "VG" at η=0.68 (Fig.25 (a)). Among the configurations with the "VG" at η=0.68, "VG η=0.2, 0.4, 0.68" presents the smallest ΔN_0, secondary is "VG η=0.2, 0.68", then "VG η=0.68" (Fig.36). The size of the "VG" has no attribute to its improvement effect.

Figure 29 shows the results of chordwise location of the vortex breakdown onset. Figure

35 show the sketches of flow pattern and smoke pictures of vortex feature on "VG η=0.68" and "VG η=0.2, 0.68". Seen from Figs.35 (a) and (c), patterns of counter-rotated vortices against inboard vortex are observed at downstream of the "VG". The area of vortex pattern also suggests that vortex generated by "VG" at η=0.68 is stronger than that by the "VG" at η=0.2 (Fig.35 (c)), because the spanwise flow becomes strong as it close to the Trailing-edge. This is why non-linear improvement effect of the "VG" at η=0.68 is conspicuous. According to Ref.8, the counter-rotated vortices are considered to reduce the effective angle of attack so that suppress flow separation and vortex breakdown. In these tests, effect of flow separation suppression is confirmed as vortex pattern reduces area of the separation region in Figs.35 (a) and (c). On the other hand, figure 29 suggests tendency of the vortex breakdown locations on each "VG" configuration is almost the same with that on the baseline except "VG η=0.2, 0.4, 0.68". This fact can lead to a conclusion that installation of "VG" does not affect inboard vortex breakdown except "VG" at η=0.4, which is in contradiction to Ref.8. However, as mentioned above, results of C_m-α indicate "VG" configurations with η=0.68 installed could improve the non-linear characteristic at (ii) which caused by vortex breakdown. Therefore the authors consider that installation of "VG" have some other influence on inboard vortex except vortex breakdown.

3.3 Relation between Non-linear Improvement and Low-Speed Aerodynamics

In order to assess the influence on low speed aerodynamic performance of each non-linear improvement device, a scatter diagram was introduced as Fig.37. The variable ΔN_0 and the maximum L/D (i.e. $(L/D)_{max}$) are set to be the x axis and y axis of the diagram, respectively. Data of all tested devices are plotted on the diagram so that their non-linear improvement effects and the L/D performance are able to be assessed simultaneously. If the plot of a device is located at upper left of the baseline, it suggests this device can simultaneously improve the non-linear characteristics and low speed aerodynamic performance. Seen from the diagram (Fig.37), the plots of the "LS" and "KS" are very close to that of the baseline. Therefore, the "LS" and "KS" have little influence on both non-linear characteristics and low-speed aerodynamics. Plots of each "VG" configurations is in general located at lower left side of the baseline, which indicate that installation of the "VG" result in a drag penalty despite of its good non-linear improvement effect. Plots of the "LE-flap" configurations are, in contrast, located at upper left side of the baseline, which means deflection of the leading-edge flap can improve both non-linear characteristics and low speed aerodynamic performance. Therefore, as a conclusion, the "LE-flap" is the most effective device to be equipped.

4 Conclusions

A series of the low speed wind tunnel testes has been conducted to understand the non-linear characteristics of the cranked-arrow wing configuration. Several devices have also been introduced to improve the non-linear characteristics. Analysis on the experimental data leads to following conclusions:

1) The non-linear characteristics are observed at two angles of attack (i.e. (i) and (ii) in Fig.19) in the range of angle of attack between 10° to 16°, which are caused by outboard flow separation and inboard vortex breakdown, respectively.
2) The non-linear characteristics are able to be improved effectively by the leading edge flap deflection and the pylon-shaped vortex generator to relevant position (i.e. η=0.68).
3) Deflection of the outboard leading-edge flap can suppress the outboard flow separation that induces the improvement of the non-linear characteristic at (i). Whereas deflection of the inboard leading-edge flap can delay the breakdown of the inboard vortex from moving toward apex of the wing. As a result improve the non-linear characteristic at (ii). Deflection of both inboard and outboard flaps can

simultaneously improve both non-linear characteristics.

4) Installation of "VG" at η=0.68 can improve non-linear characteristics at both (i) and (ii). Additional installation at η=0.2 and η=0.4 exhibit even better improvement effect.
5) The "VG" creates counter-rotated vortex against leading-edge vortex at downstream of itself. This counter-rotated vortex could reduce the effective angle of attack and suppress the flow separation if it is installed at η=0.68.
6) The LE-flap could not only improve the non-linear characteristics but also improve the maximum *L/D* of the cranked-arrow wing configuration, owing to its effect to create net thrust component. While Installation of "VG" suffers drag penalty because it increases the C_{D0} of the wing. Therefore, the present authors propose that the leading-edge flap deflection (i.e. LE-flap) is the most effective device to be used.

References

[1] Hummel D. The vortex formation over a slender wing at large angles of incidence. *AG-ARD CPP-247*, pp15.1-15.17, 1978.

[2] Hummel D. and Srinivasan P. S. Vortex breakdown effects on low speed aerodynamic characteristics of slender delta wings in symmetrical flow. *J. Royal Aeronautical Society*, Vol. 71, 1967.

[3] Liu M. J. Lu Z. Y. Qiu C. H. Su W. H. Gao X. K. Deng X. Y. and Xiong S. W. Flow patterns and aerodynamic characteristics of a wing-strake configuration. *J. Aircraft*, Vol. 17, No.5, pp 332-338, 1980.

[4] Verhaagen N. G. and Maseland J. E. J. Investigation of the vortex flow over a 76/60° double delta wing at 20 ° incidence. *AIAA-91-3208-CP*, pp 70-80, 1991.

[5] Thompson D. H. A visualization study of the vortex flow around double-delta wings. *ARL-AERO-R-165*, 1985.

[6] Brennenstuhl U. and Hummel D. Vortex Formation over Double-Delta Wings. *Proceedings of 13th Congress of the International Council of the Aeronautical Sciences (ICAS-82-6.6.3)*, Seattle, USA, Aug. 1982, pp 1144.

[7] Grafton S. B. Low-speed wind-tunnel study of the high-angle-of-attack stability and control characteristics of a cranked-arrow-wing fighter configuration. *NASA Technical Memorandum 85776*, pp1-36, May. 1984.

[8] Rao D. M. and Johnson T. D. Subsonic pitch-up alleviation on a 74° delta-wing. *NASA-CR-165749*, 1981.

[9] Rao D. M. Segmented vortex flaps. *AIAA 83-0424*, Jan. 1983.

[10] Rinoie K. Shirotake M. and Kwak D.Y. vortex behaviors of rolled supersonic transport configuration with leading-edge flaps, *J. Aircraft* Vol43, No. 6, pp1904-1916, 2006.

Copyright Statement

Fig.1 0.6m×0.6m blow-down wind tunnel in University of Tokyo

Fig.2 2m×2m low speed wind-tunnel in JAXA

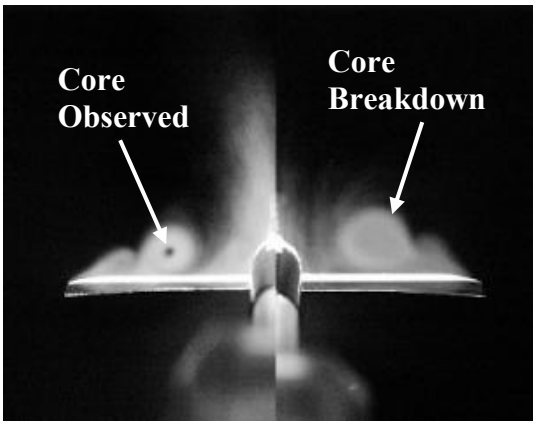

Fig.3 Vortex features over cranked-arrow wing visualized by smoke

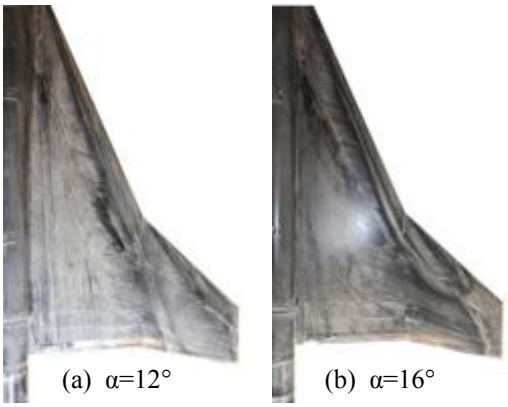

Fig.4 Oil-Flow patterns on upper surface of wing by oil flow

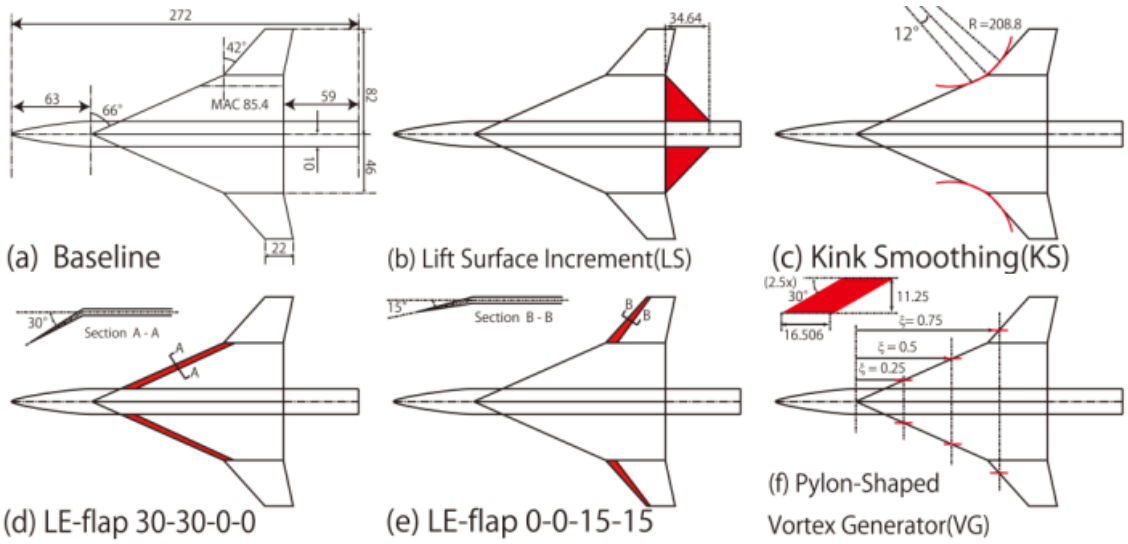

Fig.5 Schematics of the SST configurations with several aerodynamic devices equipped (wind tunnel tests in univ. of Tokyo)

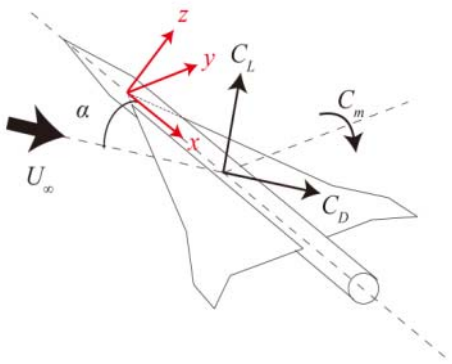

Fig.6 Definition of the orthogonal coordinate axis and aerodynamic forces

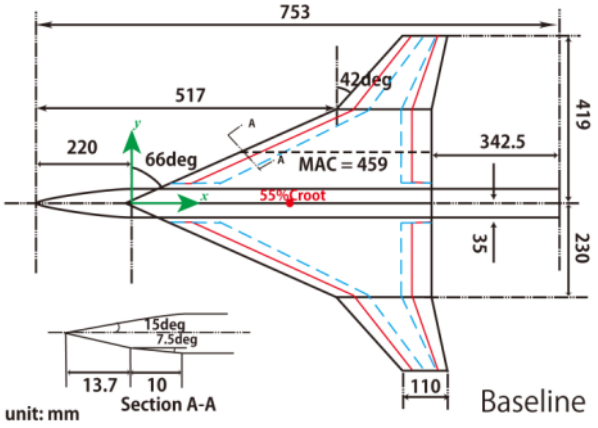

Fig.7 The baseline configuration used in JAXA wind tunnel tests

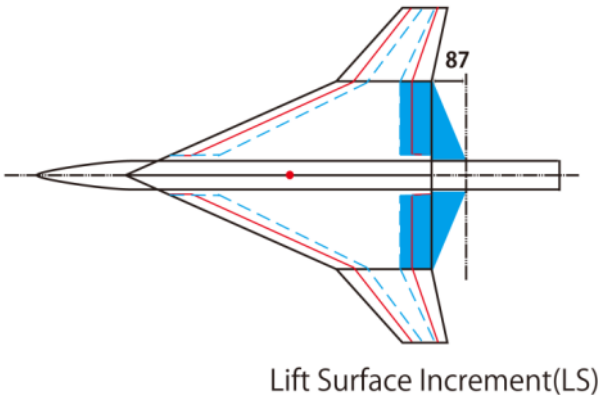

Fig.8 The "LS" configuration used in JAXA tests

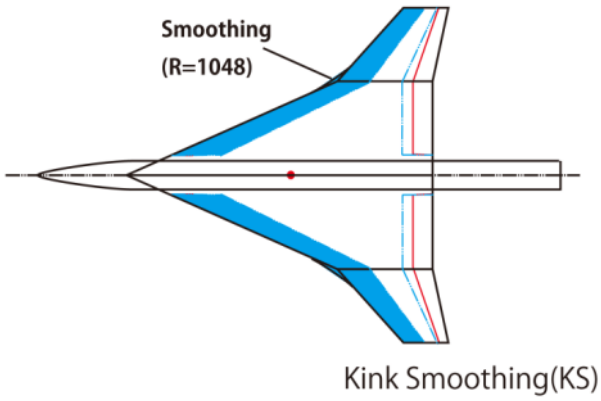

Fig.9 The "KS" configuration used in JAXA tests

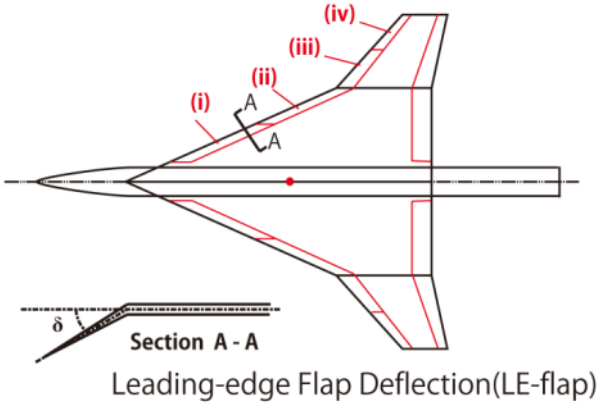

Fig.10 The "LE-flap" configuration used in JAXA tests

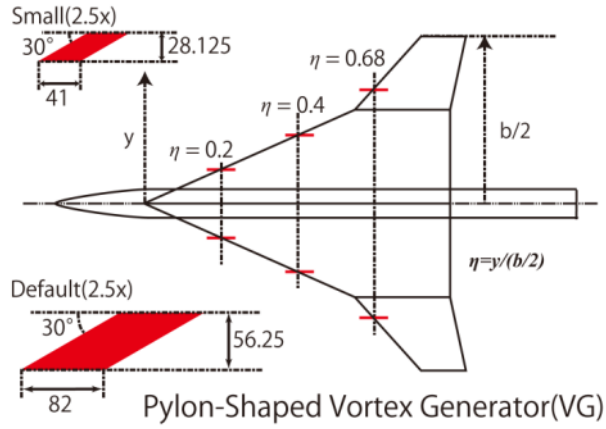

Fig.11 The "VG" configuration used in JAXA tests

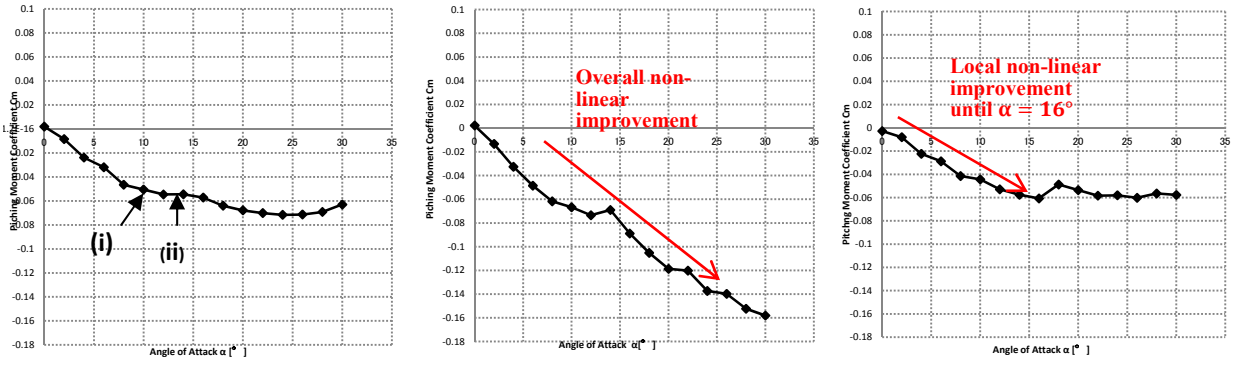

(a) Baseline (b) LS (c) KS

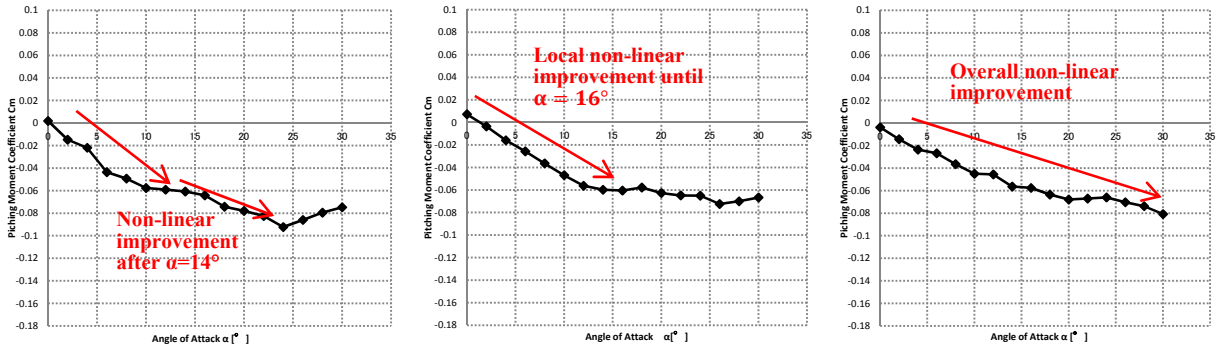

(d) LE-flap 30-30-0-0 (e) LE-flap 0-0-15-15 (f) VG

Fig.12 Pitching moment characteristics on several aerodynamic devices (Wind tunnel tests in Univ. of Tokyo)

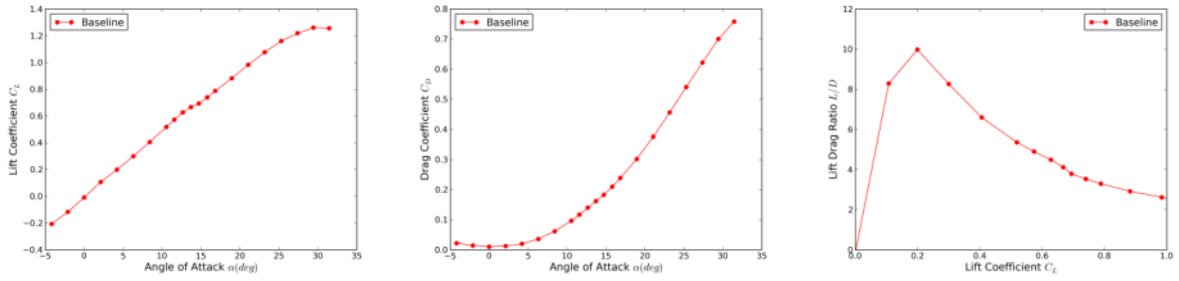

(a) C_L-α (b) C_D-α (c) L/D-C_L

Fig.13 Lift, Drag characteristics on the baseline configuration

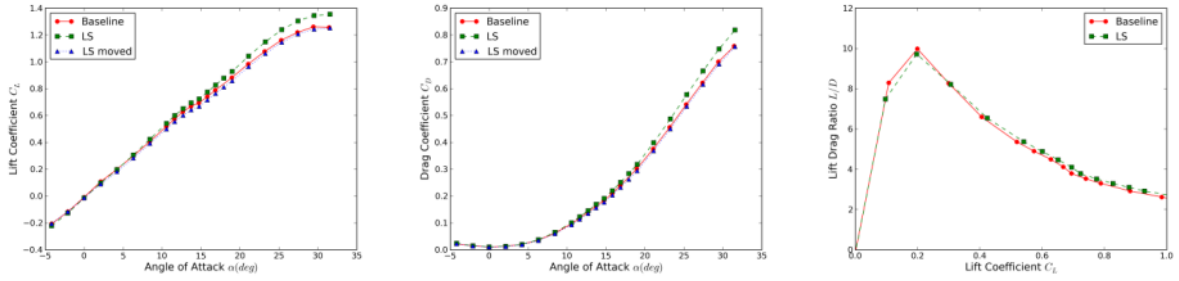

(a) C_L-α (b) C_D-α (c) L/D-C_L

Fig.14 Lift, Drag characteristics on the “LS” configuration

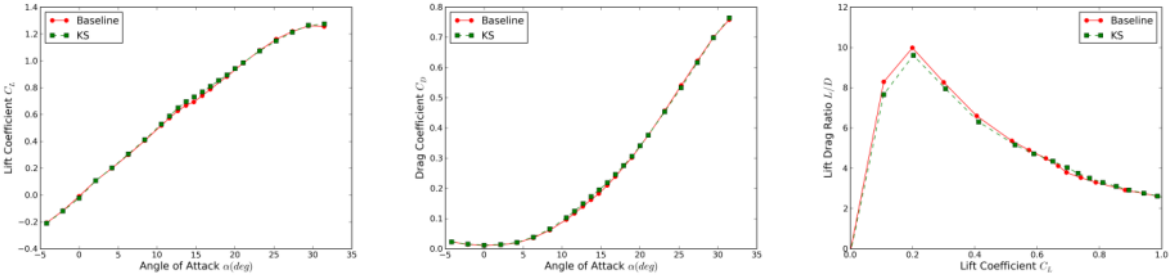

(a) C_L-α (b) C_D-α (c) L/D-C_L

Fig.15 Lift, Drag characteristics on the "KS" configuration

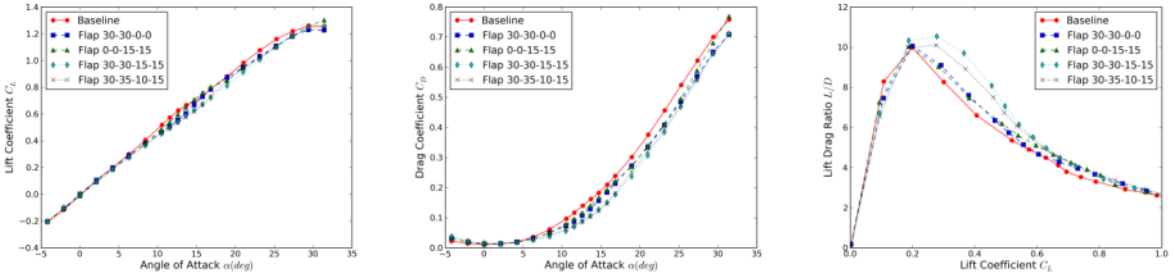

(a) C_L-α (b) C_D-α (c) L/D-C_L

Fig.16 Lift, Drag characteristics on the "LE-flap" configurations

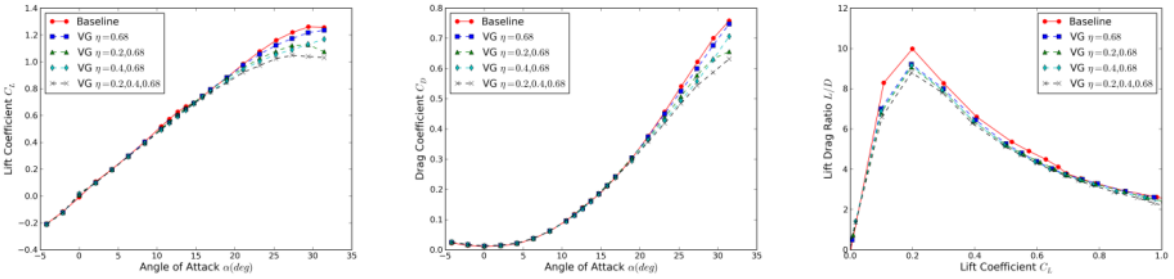

(a) C_L-α (b) C_D-α (c) L/D-C_L

Fig.17 Lift, Drag characteristics on the "VG" configurations with η=0.68 installed

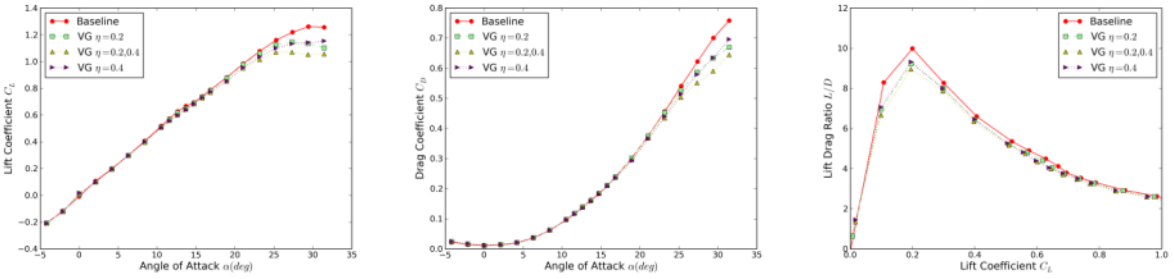

(a) C_L-α (b) C_D-α (c) L/D-C_L

Fig.18 Lift, Drag characteristics on the "VG" configurations without η=0.68 installed

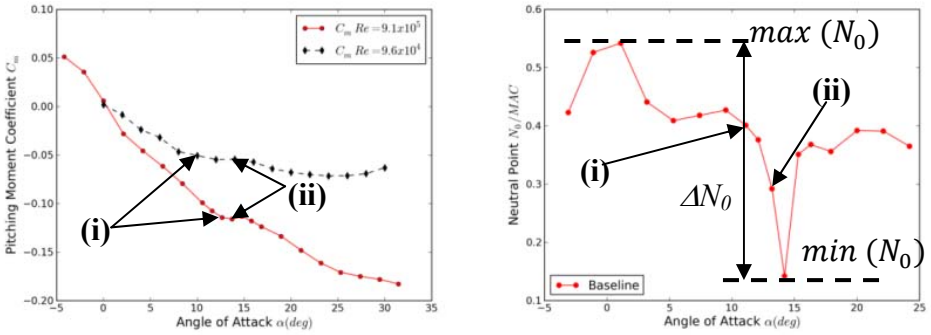

(a) C_m-α (b) N_0-α

Fig.19 Nonlinear C_m characteristics on the baseline configuration

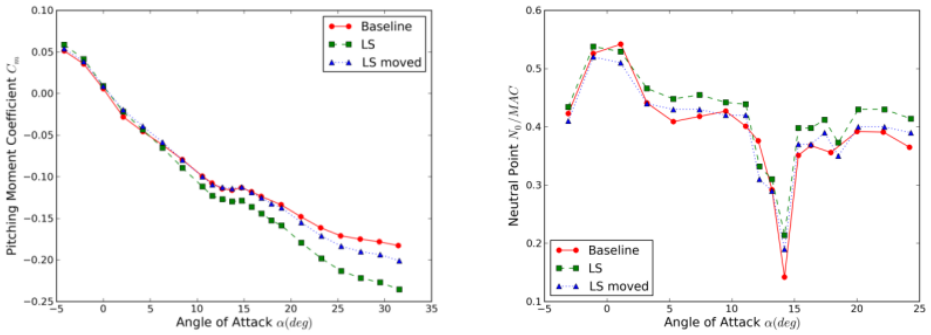

(a) C_m-α (b) N_0-α

Fig.20 Nonlinear C_m characteristics on the "LS" configuration

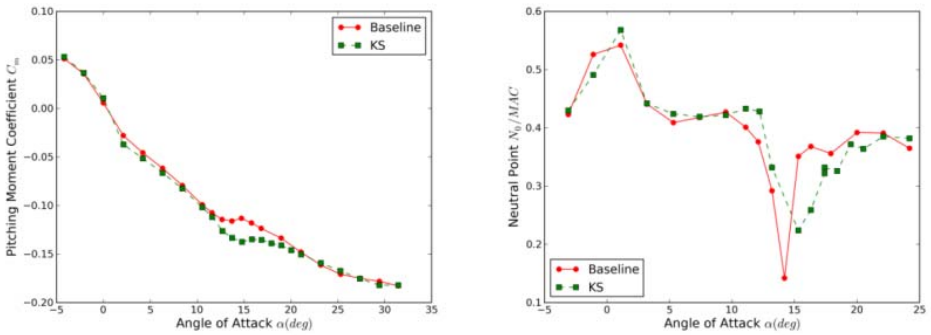

(a) C_m-α (b) N_0-α

Fig.21 Nonlinear C_m characteristics on the "KS" configuration

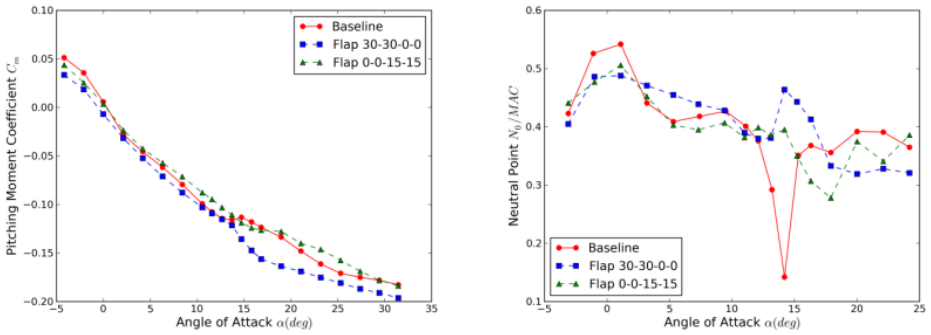

(a) C_m-α (b) N_0-α

Fig.22 Nonlinear C_m characteristics on the "LE-flap" configurations (LE-flap 30-30-0-0, 0-0-15-15)

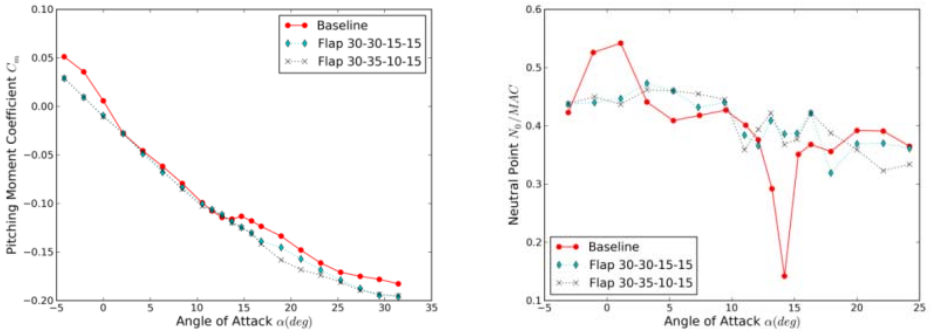

(a) C_m-α (b) N_0-α

Fig.23 Nonlinear C_m characteristics on the "LE-flap" configurations (LE-flap 30-30-15-15, 30-35-10-15)

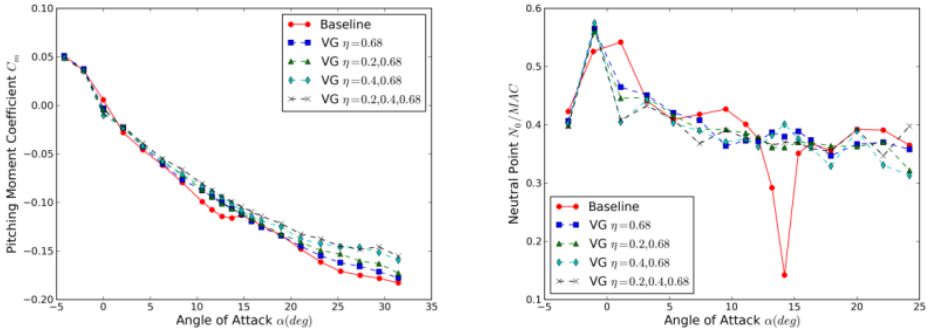

(a) C_m-α (b) N_0-α

Fig.24 Nonlinear C_m characteristics on the "VG" configurations with η=0.68 installed

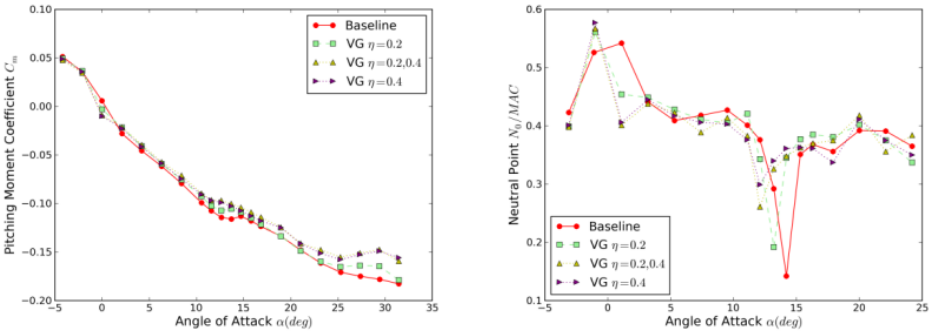

(a) C_m-α (b) N_0-α

Fig.25 Nonlinear C_m characteristics on the "VG" configurations without η=0.68 installed

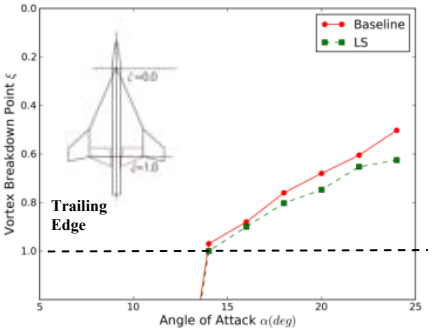

Fig.26 Chordwise locations of the inboard vortex breakdown onset on the "LS" configuration

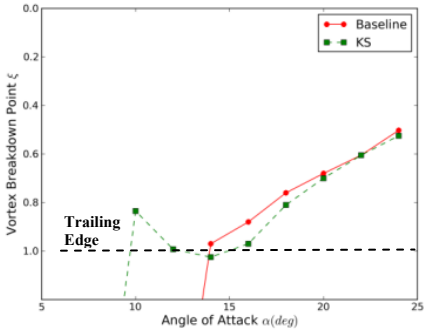

Fig.27 Chordwise locations of the inboard vortex breakdown onset on the "KS" configuration

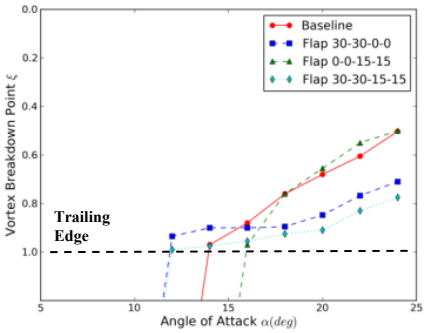

Fig.28 Chordwise locations of the inboard vortex breakdown onset on the "LE-flap" configurations

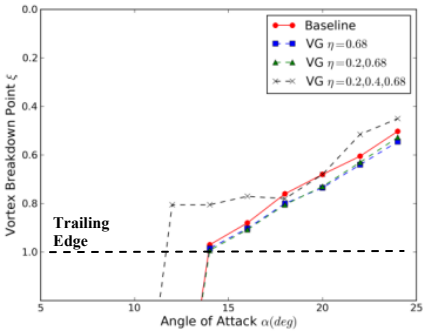

Fig.29 Chordwise locations of the inboard vortex breakdown onset on the "VG" configurations

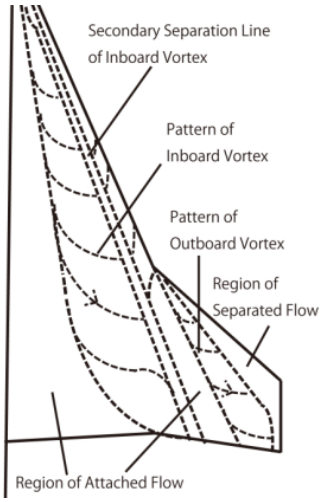

(a) α = 12°

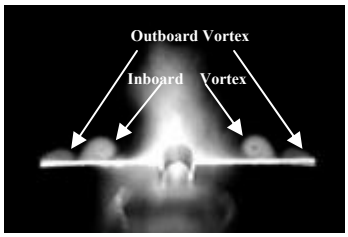

(b) α =12°
ξ =1.0

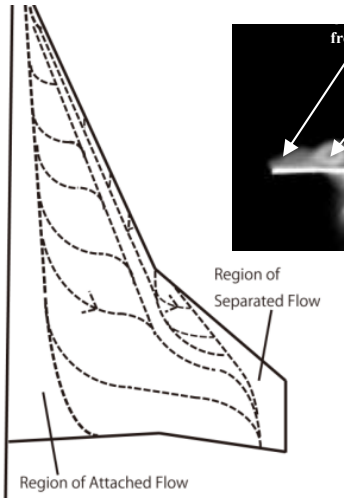

(c) α = 16°

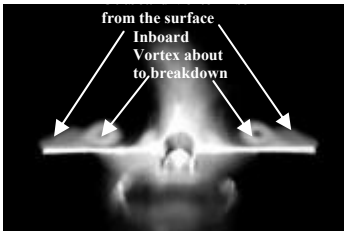

(d) α =14°
ξ =1.0

Fig.30 Surface flow pattern and vortex feature on the baseline configuration

(a) α = 16°

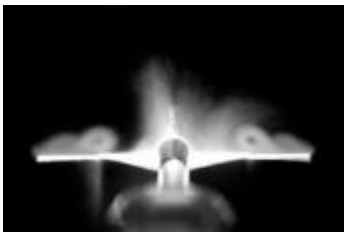

(b) α =14°
ξ =1.0

Fig.31 Surface flow pattern and vortex feature on the "LS" configuration

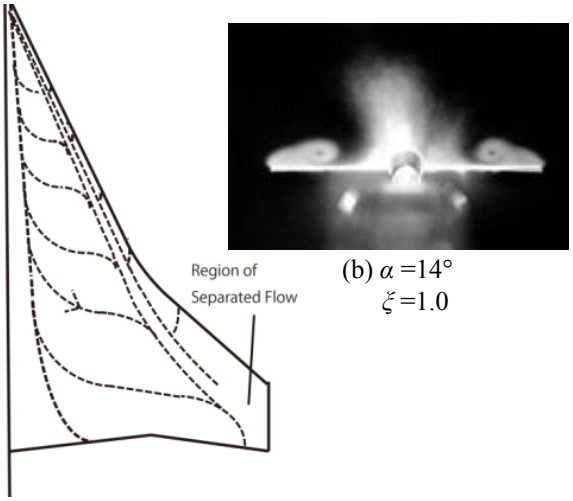

(b) α =14°
ξ =1.0

(a) α = 16°

Fig.32 Surface flow pattern and vortex feature on the "KS" configuration

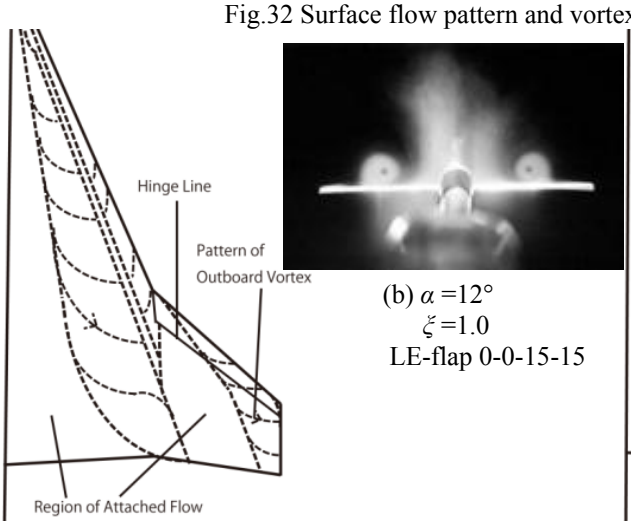

(a) α = 12°LE-flap 0-0-10-15

(b) α =12°
ξ =1.0
LE-flap 0-0-15-15

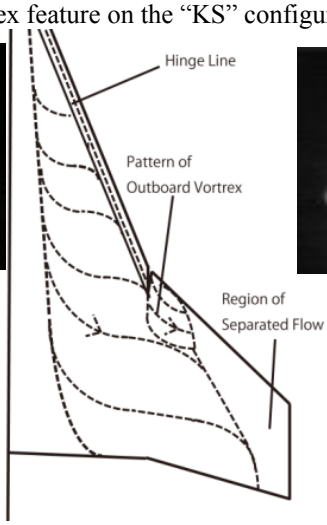

(c) α = 16° LE-flap 30-35-0-0

(d) α =16°
ξ =1.0
LE-flap 30-30-0-0

Fig.33 Surface flow pattern and vortex feature on the "LE-flap" configurations
(LE-flap 0-0-10-15, 0-0-15-15, 30-35-0-0, 30-30-0-0)

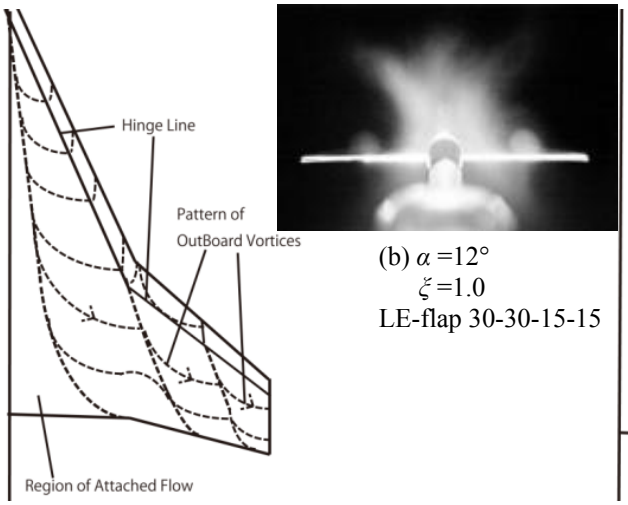

(a) α = 12°LE-flap 30-35-10-15

(b) α =12°
ξ =1.0
LE-flap 30-30-15-15

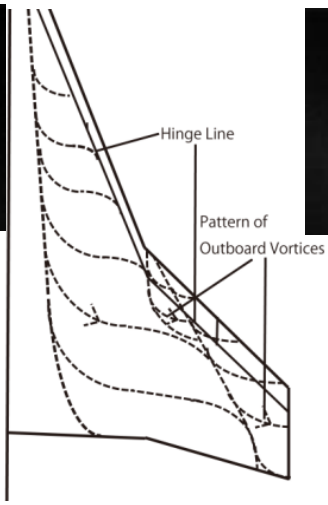

(c) α = 16° LE-flap 30-35-10-15

(d) α =16°
ξ =1.0
LE-flap 30-30-15-15

Fig.34 Surface flow pattern and vortex feature on the "LE-flap" configurations
(LE-flap 30-35-10-15, 30-30-15-15)

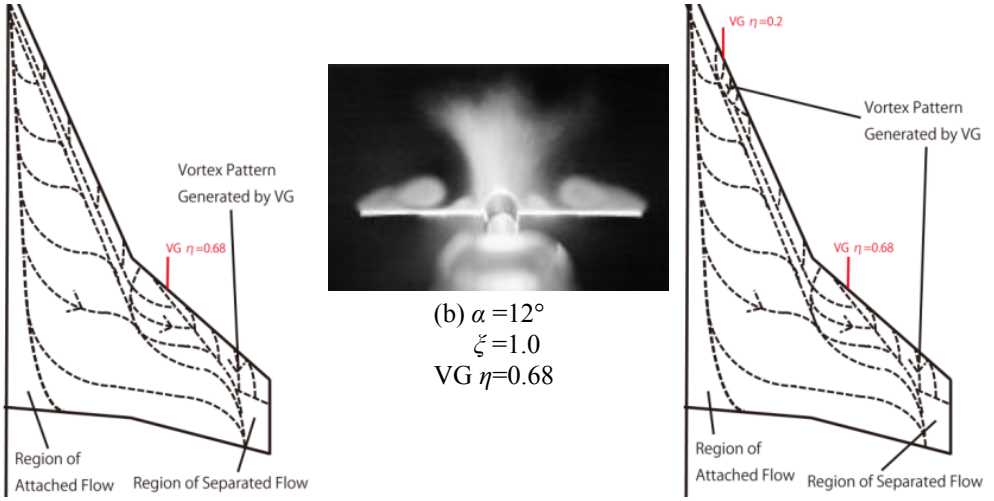

(a) α = 16°VG η = 0.68

(b) α =12°
ξ =1.0
VG η=0.68

(c) α = 16° VG η = 0.2, 0.68

Fig.35 Surface flow pattern and vortex feature on the "VG" configurations
("VG η = 0.68, "VG η = 0.2, 0.68")

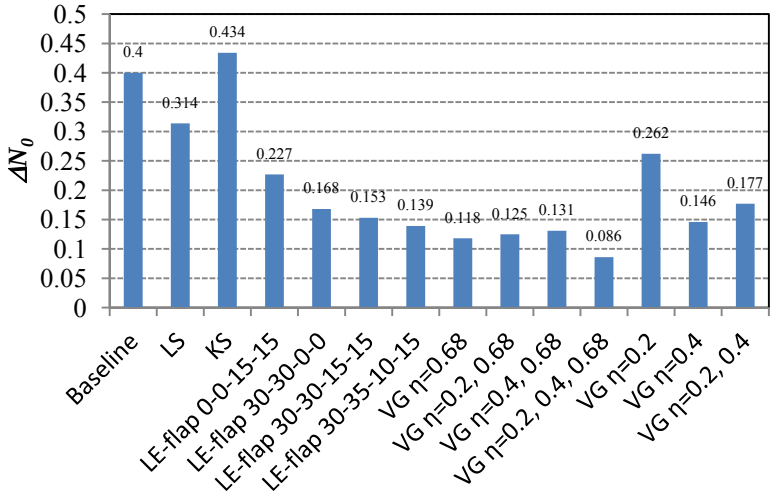

Fig.36 The ΔN_0 of several configurations

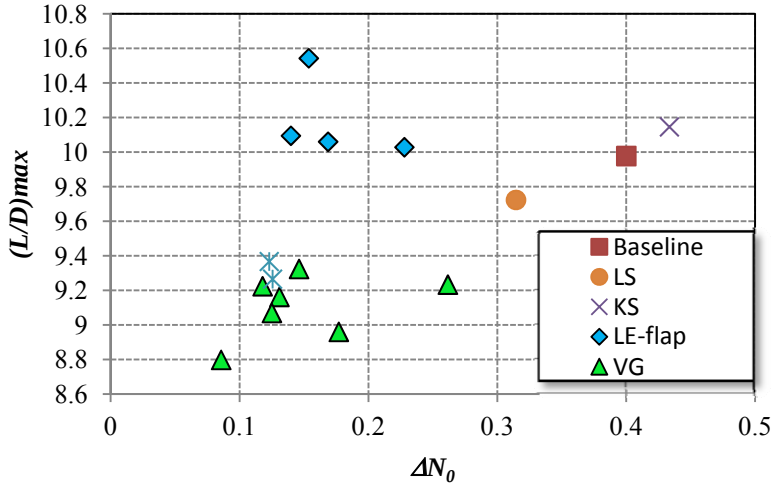

Fig.37 ΔN_0 vs $(L/D)_{max}$ scatter diagram